Controllable interatomic interaction mediated by diffractive coupling in a cavity

Ivor Krešić [*]

Centre for Advanced Laser Techniques, Institute of Physics, Bijenička Cesta 46, 10000 Zagreb, Croatia
and Institute for Theoretical Physics, Vienna University of Technology, Vienna 1040, Austria

Photon-mediated interaction can be used for simulating complex many-body phenomena with ultracold atoms coupled to electromagnetic modes of an optical resonator. We study theoretically a method of producing controllable interatomic interaction mediated by forward-diffracted photons circulating inside a ring cavity. One example of such a system is the three-mode cavity, where an on-axis mode can coexist with two diffracted sidebands. We demonstrate how the self-organized stripe states of a Bose-Einstein condensate (BEC) occurring in this cavity geometry can exhibit supersolid properties, due to spontaneous breaking of the Hamiltonian's continuous translational symmetry. A numerical study of the collective excitation spectrum of these states demonstrates the existence of massless and finite-gap excitations, which are identified as phase (Goldstone) and amplitude (Higgs) atomic density modes. We further demonstrate how judicious Fourier filtering of intracavity light can be used to engineer the effective atom-atom interaction profile for many cavity modes. The numerical results in this configuration show the existence of droplet-array and single-droplet BEC states for commensurate and incommensurate cavity modes, respectively. Diffractive coupling in a cavity is thereby introduced as an alternative route towards tailoring the photon-mediated interaction of ultracold atoms. Spatial features of the self-organized optical potentials can here be tuned to scales several times larger than the pump laser wavelength such that the corresponding atomic density distributions could be imaged and manipulated using low-numerical-aperture optics. These calculations and insights pave the way towards quantum simulation of exotic nonequilibrium many-body physics with condensates in a cavity.

I. INTRODUCTION

Ultracold atoms coupled to modes of an optical cavity can be used for simulating complex phenomena in condensed-matter physics [1,2]. The effective atom-atom interaction is here mediated by cavity photons, which has the advantage of being relatively strong and highly tunable. Throughout the past two decades, various many-body effects have been explored in this context. These include the Dicke model phase transition [3], supersolidity [4–6], and the occurrence of phonons in a quantum gas [7].

It was recently shown that diffraction of light at a cloud of cold atoms can be used to induce self-organization in atomic density [8–12] and magnetization [13–15], in the single retroreflecting mirror configuration. This type of ordering relies on the coupling between the atoms being mediated via photons diffracted by a small angle at the atomic cloud. The work on cold and ultracold atoms extends the previous theoretical ideas regarding transverse instabilities in nonlinear media [16–18], where the emphasis was placed on coupling of optical waves via the material's susceptibility.

Diffractive coupling of ultracold atoms could also be achieved using cavities, which would increase the effective strength of interactions [12,19,20]. The corresponding optical phenomena have been experimentally realized in various nonlinear media, using plano-planar cavities with intracavity lenses in the nearly self-imaging configuration, which tunes the system close to mode degeneracy [21,22]. Moreover, it was also shown that employing nearly confocal cavities can lead to the same behavior [23–25], with the potential of entering the strong cavity-medium coupling regime.

We describe here a theoretical study of the properties of diffractive coupling in a one-dimensional Bose-Einstein condensate (BEC) coupled to electromagnetic modes of a ring cavity. We demonstrate how the profile of the photon-mediated atom-atom interaction can be tailored by filtering the Fourier modes to allow propagation of light with desired transverse wavelengths. Within the mean-field approximation, laser driving of the on-axis cavity mode can lead to BEC self-organization into stripe states for a setup with two cavity sidebands. We explore the supersolid properties of these stripe states arising due to spontaneous breaking of the U(1) translational symmetry of the system Hamiltonian. The Bogoliubov theory calculation reveals the presence of phase (Goldstone) and amplitude (Higgs) modes in atomic density. In the case of many cavity modes, we numerically demonstrate the existence of droplet arrays and single-droplet states for commensurate and incommensurate cavity sidebands, respectively.

Methods of controlling the cavity-photon-mediated interaction were recently implemented in cold atoms in a single-mode cavity with an applied magnetic-field gradient [26], along with ultracold atoms coupled to modes of a multimode degenerate cavity [27]. Another theoretically proposed

---

[*]Contact author: ikresic@ifs.hr

method relies on using frequency combs for pumping a BEC near cavity resonances of multiple longitudinal cavity modes [28]. The present article describes an addition to the toolbox for control of photon-mediated interaction profiles in quantum simulations. The great advantage compared to the methods of Refs. [26–28] is that the allowed cavity-mode wave vectors can be selected with considerable freedom such that, e.g., modes with incommensurate transverse wavelengths can be excited, leading to complex dynamics.

Another advantage stems from the fact that the self-organization mechanism does not rely on collective superradiant enhancement of scattering into an optical cavity mode orthogonal to the pump laser [29] and the spatial period of the patterns can be made several times larger than the pump wavelength. Experimental realization of BEC self-organization at such length scales would offer considerable advantages in terms of optical control and monitoring of the system dynamics as compared to the superradiant cases described in [1,2], where the spatial periods are near the diffraction limit.

II. SYSTEM HAMILTONIAN

The setup consists of a BEC placed inside a nearly degenerate ring cavity, with a laser of frequency ω driving an on-axis cavity mode with pump rate η. For strong BEC confinement along the y and z axes, the cloud has a cigar shape and can be approximated as one dimensional. Moreover, for pattern length scales several times larger than the light's wavelength, the paraxial approximation holds and the reflection of intracavity light from the BEC can be neglected, i.e., only diffracted waves at a small angle to the pump beam direction are considered.

Using the Fourier filtering technique for photons inside the cavity [15,30], one can tailor the configuration of the allowed cavity sideband modes. The cavity operator is then given by

$$\hat{E}(x) = \hat{a}_0 + \sum_{q_j \in S} (\hat{a}_{j+} e^{iq_j x} + \hat{a}_{j-} e^{-iq_j x}), \quad (1)$$

where $\hat{a}_0$ is the annihilation operator of the on-axis mode and $\hat{a}_{j\pm}$ are the annihilation operators of the diffracted sideband modes with transverse wave numbers $\pm q_j = \pm 2\pi/\Lambda_j$. The sum goes over q_j values belonging to a discrete and finite set S.

The effective many-body Hamiltonian for the atomic and cavity degrees of freedom can be derived from the Jaynes-Cummings model, as described in Appendix A. This effective Hamiltonian has the form ($\hbar = 1$)

$$\hat{H}_{\text{eff}} = -\Delta_c \hat{a}_0^\dagger \hat{a}_0 - \sum_j \Delta_{c,j} (\hat{a}_{j+}^\dagger \hat{a}_{j+} + \hat{a}_{j-}^\dagger \hat{a}_{j-}) + i\eta(\hat{a}_0^\dagger - \hat{a}_0)$$
$$+ \int \hat{\psi}^\dagger(x) \left(-\frac{1}{2m} \frac{\partial^2}{\partial x^2} + V_1(x) + U_0 \hat{E}^\dagger(x) \hat{E}(x) \right)$$
$$\times \hat{\psi}(x) dx, \quad (2)$$

where $\hat{\psi}(x)$ is the atomic field operator, $V_1(x)$ is the external potential, m is the mass of an atom, $\Delta_c = \omega - \omega_0$ and $\Delta_{c,j} = \omega - \omega_{c,j}$ are the pump detunings from the on-axis and jth sideband cavity mode, respectively, $U_0 = g_0^2/\Delta_a$ is the single-atom light shift, $\Delta_a = \omega - \omega_a$ is the laser-atom detuning, and

g_0 is the atom-cavity coupling strength. The number of atoms N in the following calculations is kept constant throughout the dynamical evolution.

The Hamiltonian describing the effective atom-atom interaction mediated by diffractive coupling via the cavity photons is given by

$$\hat{H}_{\text{eff,at}} = \int \hat{\psi}^\dagger(x) \left(-\frac{1}{2m} \frac{\partial^2}{\partial x^2} + V_1(x) \right) \hat{\psi}(x) dx$$
$$+ \frac{1}{2} \int \hat{\psi}^\dagger(x') \hat{\psi}^\dagger(x) V_2(x, x') \hat{\psi}(x) \hat{\psi}(x') dx dx', \quad (3)$$

where the effective atom-atom interaction is given by

$$V_2(x, x') = \frac{4U_0^2 \eta^2}{\bar{\Delta}_c^2 + \kappa^2} \sum_{q_j \in S} \frac{\bar{\Delta}_{c,j}}{\bar{\Delta}_{c,j}^2 + \kappa^2} \cos[q_j(x - x')], \quad (4)$$

with $\bar{\Delta}_c = \omega - \omega_0 - NU_0$ and $\bar{\Delta}_{c,j} = \omega - \omega_{c,j} - NU_0$. The effective atom-atom interaction $V_2(x, x')$ can thus be controlled by Fourier filtering to select a desired set of modes S.

In the following, we first explore the simple case of two cavity sidebands, where global all-to-all coupling between the atoms occurs. We demonstrate how such a setup can be used to simulate the phenomenon of supersolidity. We extend these studies to a multimode situation with eight cavity sidebands, which enables us to explore the relationship between commensurability of the cavity modes and the atomic ground-state solution.

III. SUPERSOLID PROPERTIES OF SELF-ORGANIZED STRIPE STATES

Supersolids are an intriguing phase of matter with coexisting spatial order and superfluidity. The phenomenon has been studied theoretically over the past 50 years [31–37]; however, conclusive experimental observations in the context of condensed-matter physics are still lacking [38,39].

Several experiments have recently shown that novel insights into supersolidity can be gleaned by quantum simulation with ultracold atoms [2,40,41]. For a Bose-Einstein condensate (BEC), the global U(1) phase symmetry is spontaneously broken by condensation [42], and spontaneous breaking of the continuous spatial (translational and/or rotational) symmetry via crystallization can lead to supersolidity. The types of interactions employed for simulating supersolidity in BECs range from cavity-photon-mediated [4,6,7,28,43,44] and strong magnetic dipolar [45–51] to synthetic spin-orbit coupling [52]. Although such analog systems provide only simplified versions of the actual interactions present in condensed-matter materials, their study can add valuable insight into the properties of the elusive supersolid phase [43].

Below we study photon-mediated supersolidity of the self-organized stripe states in the ring cavity setup, depicted in Fig. 1(a). The cavity operator is now given by

$$\hat{E}_{\text{st}}(x) = \hat{a}_0 + \hat{a}_+ e^{iq_c x} + \hat{a}_- e^{-iq_c x}, \quad (5)$$

where $\hat{a}_0$ is the on-axis mode and $\hat{a}_\pm$ are the sideband mode photonic annihilation operators. The two sidebands
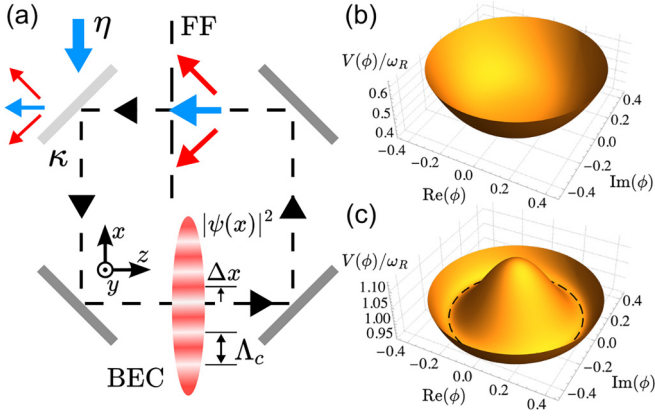
FIG. 1. Self-organization and supersolidity in the configuration with three cavity modes. (a) An effectively one-dimensional ultracold Bose-Einstein condensate is placed inside a ring cavity with a linewidth κ, which is pumped by coherent on-axis light with drive amplitude η (blue arrow). A Fourier filtering (FF) stage ensures propagation of only three cavity modes. Upon self-organization, the BEC density distribution $|\psi(x)|^2$ orders into a stripe pattern with a pattern phase displacement Δx, which can be defined as the distance of the first maximum from the origin $x = 0$. The value of Δx is selected via spontaneous symmetry breaking for a particular pattern realization and depends on the atomic sideband phase $\arg\phi$. The pattern length scale Λ_c is tunable via Fourier filtering. The effective potential for the atoms $V(\phi)$ as a function of the complex parameter ϕ has (b) a circular paraboloid shape at laser pump strengths below the self-organization threshold ($\eta = 0.9\eta_c$) and (c) a sombrero shape above threshold ($\eta = 1.5\eta_c$), which is a direct consequence of the U(1) translational symmetry of the system Hamiltonian. The dashed line indicates the potential minima at $|\phi_0| = 0.373$. The other parameters are $(\bar{\Delta}_c, \bar{\Delta}'_c, u_0) = (2, -1, -1)\omega_R$.

have transverse wave numbers $\pm q_c = \pm 2\pi/\Lambda_c$ and detunings $\Delta'_c = \omega - \omega'_0$.

The many-body Hamiltonian is here given by

$$\hat{H}_{\text{st}} = \hat{H}_{\text{ph,st}} + \int \hat{\psi}^\dagger(x)\hat{H}^{(1)}_{\text{at,st}}\hat{\psi}(x)dx, \qquad (6)$$

where $\hat{H}_{\text{ph,st}} = -\Delta_c\hat{a}^\dagger_0\hat{a}_0 - \Delta'_c(\hat{a}^\dagger_+\hat{a}_+ + \hat{a}^\dagger_-\hat{a}_-) + i\eta(\hat{a}^\dagger_0 - \hat{a}_0)$ and the single-atom Hamiltonian is given by

$$\hat{H}^{(1)}_{\text{at,st}} = -\frac{1}{2m}\frac{\partial^2}{\partial x^2} + U_0[\hat{a}^\dagger_0\hat{a}_0 + \hat{a}^\dagger_+\hat{a}_+ + \hat{a}^\dagger_-\hat{a}_- + (\hat{a}^\dagger_0\hat{a}_+$$
$$+ \hat{a}^\dagger_-\hat{a}_0)e^{iq_cx} + (\hat{a}^\dagger_0\hat{a}_- + \hat{a}^\dagger_+\hat{a}_0)e^{-iq_cx} + \hat{a}^\dagger_-\hat{a}_+e^{2iq_cx}$$
$$+ \hat{a}^\dagger_+\hat{a}_-e^{-2iq_cx}]. \qquad (7)$$

Note that $\hat{H}_{\text{st}}$ is symmetric to continuous translations by distance d along the x axis, i.e., transformations of the form $\hat{\psi}(x) \to \hat{\psi}(x+d)$ and $\hat{E}(x) \to \hat{E}(x+d)$. In the thermodynamic mean-field limit, the continuous translational symmetry is spontaneously broken by the system selecting a random relative phase between the cavity sideband modes, and the phase of the periodic atomic density distribution. Note that in this case $V_2(x, x')$ varies spatially as $\cos[q_c(x - x')]$. This is analogous to the case of superradiant self-organization in a ring cavity [44].

Simultaneous breaking of the global U(1) phase symmetry by Bose-Einstein condensation [42] and the U(1) translational symmetry by photon-mediated structuring into a density pattern means that the self-organized state of the BEC can display supersolid properties [43], as studied below. For the fully quantum description, this U(1) translational symmetry of $\hat{H}_{\text{st}}$ leads to the preservation of transverse momentum of photons and atoms by the nonlinear scattering processes, which in the transient regime can lead to quantum correlations [53].

A. Three-mode optomechanical model

In the three-mode optomechanical model [54], the $\hat{\psi}(x)$ for this setup given is by

$$\hat{\psi}(x) = \frac{1}{\sqrt{L}}(\hat{b}_0 + \hat{b}_+e^{iq_cx} + \hat{b}_-e^{-iq_cx}), \qquad (8)$$

where $\hat{b}_j$ is the bosonic annihilation operator of the jth transverse atomic momentum mode and L is the length of the one-dimensional cloud. Inserting relations (5) and (8) into (6) and performing the integration over the BEC cloud length L, one obtains the three-mode Hamiltonian $\hat{H}_{3M} = \hat{H}_0 + \hat{H}_{\text{FWM}}$. The noninteracting part is $\hat{H}_0 = -\bar{\Delta}_c\hat{a}^\dagger_0\hat{a}_0 - \bar{\Delta}'_c(\hat{a}^\dagger_+\hat{a}_+ + \hat{a}^\dagger_-\hat{a}_-) + \omega_R(\hat{b}^\dagger_+\hat{b}_+ + \hat{b}^\dagger_-\hat{b}_-) + i\eta(\hat{a}^\dagger_0 - \hat{a}_0)$, where $\bar{\Delta}_c = \Delta_c - NU_0$, $\bar{\Delta}'_c = \Delta'_c - NU_0$, and $\omega_R = q_c^2/2m$ is the transverse photon-recoil energy, while the four-wave mixing part $\hat{H}_{\text{FWM}}$ has the form

$$\hat{H}_{\text{FWM}} = U_0[(\hat{a}^\dagger_+\hat{b}^\dagger_- + \hat{a}^\dagger_-\hat{b}^\dagger_+)\hat{a}_0\hat{b}_0 + \hat{a}^\dagger_0(\hat{b}^\dagger_+\hat{a}_+ + \hat{b}^\dagger_-\hat{a}_-)\hat{b}_0$$
$$+ \hat{a}^\dagger_+\hat{a}_-\hat{b}^\dagger_-\hat{b}_+] + \text{H.c.} \qquad (9)$$

The details of the derivation of the Hamiltonian $\hat{H}_{3M}$ are given in [53].

We now derive the expression for the expectation value of the Hamiltonian, also called the effective potential $V(\phi)$ for a complex order parameter ϕ [5,48,55], from the microscopic Hamiltonian $\hat{H}_{3M}$ in the mean-field thermodynamic limit, where $\langle\hat{O}_1\hat{O}_2\hat{O}_3\hat{O}_4\rangle \to \langle\hat{O}_1\rangle\langle\hat{O}_2\rangle\langle\hat{O}_3\rangle\langle\hat{O}_4\rangle$.

Writing $\langle\hat{a}_j\rangle \to \sqrt{N}\alpha_j$ and $\langle\hat{b}_j\rangle \to \sqrt{N}\beta_j$ and neglecting the fourth-order terms in the sidebands, which is justified near the self-organization threshold, one can calculate the energy in the photon-atom system in the mean-field limit

$$\langle\hat{H}_{3M}\rangle/N = -\bar{\Delta}_c|\alpha_0|^2 - \bar{\Delta}'_c(|\alpha_+|^2 + |\alpha_-|^2) + i\frac{\eta}{\sqrt{N}}(\alpha_0^* - \alpha_0)$$
$$+ \omega_R(|\beta_+|^2 + |\beta_-|^2) + u_0[\alpha_0\beta_0(\alpha_+^*\beta_-^* + \alpha_-^*\beta_+^*)$$
$$+ \alpha_0^*\beta_0(\alpha_+\beta_+^* + \alpha_-\beta_-^*) + \text{c.c.}], \qquad (10)$$

with $u_0 = NU_0$. As $|\bar{\Delta}_c|, |\bar{\Delta}'_c| \gg \omega_R$, the photonic degrees of freedom adiabatically follow the atomic ones, and by setting $\frac{\partial\langle\hat{H}_{3M}\rangle}{\partial\alpha_i^*} = 0$ we adiabatically eliminate them to get

$$\alpha_0 = \frac{i\eta}{\sqrt{N}\bar{\Delta}_c}, \qquad \alpha_\pm = \frac{u_0}{\bar{\Delta}'_c}\alpha_0\beta_0(\beta_\pm + \beta_\mp^*), \qquad (11)$$

where we have chosen a real-valued $\beta_0 = \sqrt{1 - |\beta_+|^2 - |\beta_-|^2}$, while for α_0 we have neglected the terms proportional to $\frac{u_0}{\bar{\Delta}'_c}\alpha_\pm^{(*)}\beta_\pm^{(*)}$, as $|u_0| \ll |\bar{\Delta}'_c|$ and η is near the self-organization threshold. Writing $\frac{\partial\langle\hat{H}_{3M}\rangle}{\partial\beta_\pm} = 0$, one finds that in equilibrium $\beta_+ = \beta_-^*$.

We now introduce the complex mean-field order parameter $\phi = \phi_1 + i\phi_2 = \beta_+ = \beta_-^*$. Inserting the relations (11) into the expression (10), one finds that the effective potential $V(\phi) = \langle \hat{H}_{3M} \rangle_{eq}/N$ is rotationally symmetric and has a Coleman-Weinberg form [56–58] for a homogeneous (long-wavelength) order parameter ϕ, given by

$$V(\phi) = h_0 + h_1 |\phi|^2 + \frac{h_2}{2} |\phi|^4, \quad (12)$$

with the parameters

$$h_0 = \frac{\eta^2}{N\bar{\Delta}_c}, \quad h_1 = 2\omega_R \left(1 - \frac{\eta^2}{\eta_c'^2} \right), \quad h_2 = 8\omega_R \frac{\eta^2}{\eta_c'^2}, \quad (13)$$

where the critical pump strength η_c' is given by $\eta_c' = \sqrt{-\omega_R \bar{\Delta}_c' \bar{\Delta}_c^2 / 4NU_0^2}$. Note that η_c' is equal to the critical pump strength η_c [53],

$$\eta_c = \sqrt{\frac{-\omega_R (\bar{\Delta}_c^2 + \kappa^2)(\bar{\Delta}_c'^2 + \kappa^2)}{4NU_0^2 \bar{\Delta}_c'}}, \quad (14)$$

for vanishing cavity-photon decay rate κ. As show in Figs. 1(c) and 1(d), for $h_1 > 0$ ($\eta < \eta_c'$), $V(\phi)$ is a paraboloid, while for $h_1 < 0$ ($\eta > \eta_c'$) it deforms into a sombrero shape, with minima at $|\phi| = \phi_0$, where

$$\phi_0 = \sqrt{-\frac{h_1}{h_2}} = \frac{1}{2} \sqrt{1 - \frac{\eta_c'^2}{\eta^2}}. \quad (15)$$

The sombrero shape of $V(\phi)$ above the self-organization threshold is a direct consequence of the continuous translational symmetry of the Hamiltonian. After spontaneous breaking of this U(1) translational symmetry, the system Hamiltonian can support the existence of two collective excitations: one gapless related to fluctuations at constant $|\phi|$ (Goldstone or phase mode) and one with a finite-energy gap related to fluctuations at a constant $\arg \phi$ (Higgs or amplitude mode) [5,48,55]. The simultaneous presence of Goldstone and Higgs modes is characteristic of supersolidity and is determined below by calculating the collective excitation spectrum using Bogoliubov–de Gennes theory.

The dynamical equations for the cavity photons and the three atomic modes can be calculated by considering the Lindblad-like evolution equations for the photon mode fields $\alpha_0(t)$ and $\alpha_\pm(t)$ and the Heisenberg equation for the three atomic motional modes $\beta_0(t)$ and $\beta_\pm(t)$, which leads to [53]

$$\frac{\partial \alpha_0}{\partial t} = (i\bar{\Delta}_c - \kappa)\alpha_0 - iu_0[(\beta_+^* \alpha_+ + \beta_-^* \alpha_-)\beta_0$$
$$+ \beta_0^*(\alpha_+ \beta_- + \alpha_- \beta_+)] + \frac{\eta}{\sqrt{N}},$$

$$\frac{\partial \alpha_\pm}{\partial t} = (i\bar{\Delta}_c' - \kappa)\alpha_\pm - iu_0[(\beta_\mp^* \beta_0 + \beta_0^* \beta_\pm)\alpha_0 + \alpha_\mp \beta_\mp^* \beta_\pm] \quad (16)$$

and

$$\frac{\partial \beta_0}{\partial t} = -iu_0[\alpha_0^*(\alpha_+ \beta_- + \alpha_- \beta_+) + (\alpha_+^* \beta_+ + \alpha_-^* \beta_-)\alpha_0)],$$

$$\frac{\partial \beta_\pm}{\partial t} = -i\omega_R \beta_\pm - iu_0[(\alpha_\mp^* \alpha_0 + \alpha_0^* \alpha_\pm)\beta_0 + \alpha_\mp^* \alpha_\pm \beta_\mp]. \quad (17)$$
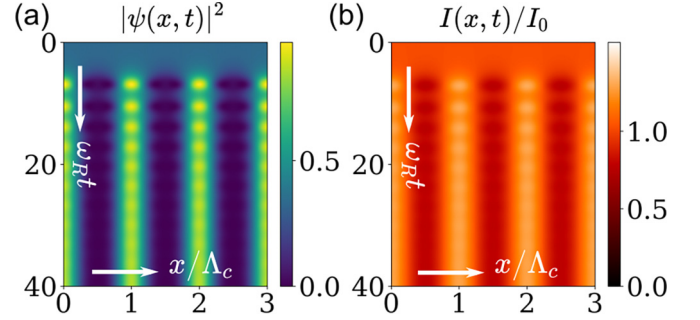

FIG. 2. Dynamical evolution after switching on the pump laser for (a) the atomic probability density $|\psi(x,t)|^2$ and (b) the electric-field intensity profile $I(x,t)$, normalized to the steady-state value of the on-axis mode intensity $I_0 = |\alpha_0^0|^2$. The on-axis intracavity field initially grows on the scale of approximately $1/\kappa$ (not discernible) and approximately reaches its steady-state value α_0^0. This homogeneous solution is not stable and stripe patterns begin to form, with the system undergoing sloshing oscillations before reaching the steady state, where the atoms are bunched into maxima of light intensity, due to $\Delta_a < 0$. The phase of the self-organized pattern was set to 0 for clarity, but can attain any value between 0 and 2π due to continuous translational symmetry of $\hat{H}_{eff}$. The simulation parameters are $\eta = 1.5\eta_c$ and $(\bar{\Delta}_c, \bar{\Delta}_c', u_0, \kappa) = (10, -5, -1, 5)\omega_R$.

These equations can be used to study the dynamics of the system near the instability threshold η_c.

In Fig. 2 we plot the temporal evolution of atomic probability distribution along the x axis, given by $|\psi(x,t)|^2 = |\beta_0(t) + \beta_+(t)\exp(iq_c x) + \beta_-(t)\exp(-iq_c x)|^2/L$, and the photon field profile, given by the intensity $I(x,t) = |\alpha_0(t) + \alpha_+(t)\exp(iq_c x) + \alpha_-(t)\exp(-iq_c x)|^2$, calculated by solving Eqs. (16) and (17). After switching on the pump laser at $t = 0$, the atomic probability distribution is homogeneous and the α_0 quickly increases to approximately its steady-state value after a time $1/\kappa$. This homogeneous solution soon becomes unstable and the stripe pattern begins to form. At the onset of the instability, the system undergoes sloshing motion, marked by continuous oscillation between the bunched and homogeneous atomic and electric-field pattern, studied, e.g., in [59]. After the oscillations decay, a striped steady state is reached, with atoms bunching into the peaks of the electric-field intensity due to the drive being red detuned from the optical transition of the atoms, i.e., $U_0 < 0$.

B. Gross-Pitaevskii-type equation

Following the approach of [44,60], here we move away from the three-mode model, which leads to equations of the Gross-Pitaevskii type for the atomic wave function. Using the same approximations as above with the Hamiltonian $\hat{H}_{st}$, we get the dynamical equations for the photon mode fields $\alpha_0(t)$ and $\alpha_\pm(t)$ and atomic wave function $\psi(x,t)$,

$$\frac{\partial \alpha_0}{\partial t} = (i\bar{\Delta}_c - \kappa)\alpha_0 - iu_0(\alpha_+ \mathcal{I}_+ + \alpha_- \mathcal{I}_-) + \frac{\eta}{\sqrt{N}},$$

$$\frac{\partial \alpha_\pm}{\partial t} = (i\bar{\Delta}_c' - \kappa)\alpha_\pm - iu_0(\alpha_0 \mathcal{I}_\mp + \alpha_\mp \mathcal{I}_{2\mp}),$$

$$i\frac{\partial \psi}{\partial t} = -\frac{1}{2m}\frac{\partial^2 \psi}{\partial x^2} + u_0[|\alpha_0|^2 + |\alpha_+|^2 + |\alpha_-|^2$$

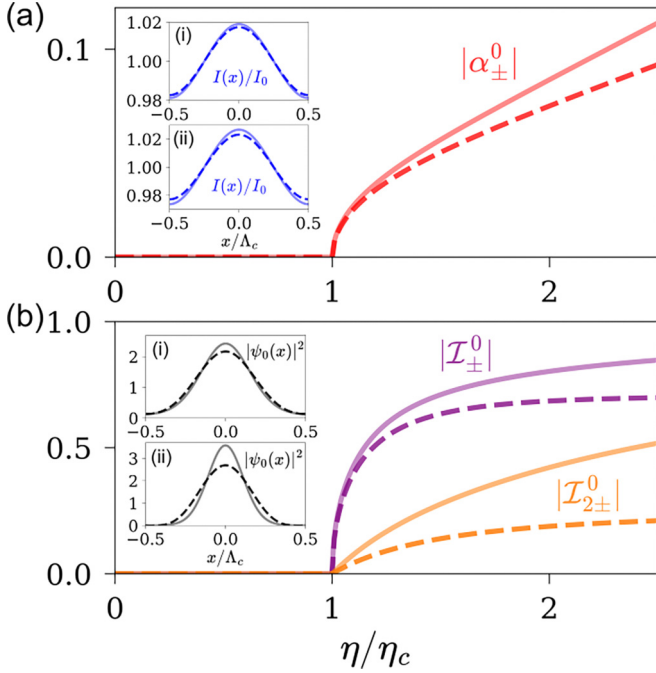FIG. 3. Steady-state values of (a) $|\alpha_\pm^0|$ and (b) $|\mathcal{I}_\pm^0|$ and $|\mathcal{I}_{2\pm}^0|$ versus η. The insets depict the (a) intracavity electric-field intensity $I(x)/I_0$ and (b) probability distribution $|\psi_0(x)|^2$, where in (i) $\eta = 1.2\eta_c$ and in (ii) $\eta = 1.8\eta_c$, with the phase of the self-organized pattern set to 0 for clarity. The solid lines in all plots represent the results for the steady-state solutions of Eqs. (18), while the dashed lines are for the solutions of the three-mode model, where $\mathcal{I}_\pm^0 = \beta_\mp^0(\beta_0^0)^* + \beta_0^0(\beta_\pm^0)^*$ and $\mathcal{I}_{2\pm}^0 = \beta_\mp^0(\beta_\pm^0)^*$. The simulation parameters are $(\bar{\Delta}_c, \bar{\Delta}_c', u_0, \kappa) = (119, -89, -1, 50)\omega_R$.

$$
\begin{aligned}
&+ (\alpha_0^*\alpha_- + \alpha_+^*\alpha_0)e^{-iq_cx} + \alpha_+^*\alpha_- e^{-2iq_cx} \\
&+ (\alpha_0^*\alpha_+ + \alpha_-^*\alpha_0)e^{iq_cx} + \alpha_-^*\alpha_+ e^{2iq_cx}]\psi, \qquad (18)
\end{aligned}
$$

where the integrals $\mathcal{I}_\pm = \int e^{\pm iq_cx}|\psi(x,t)|^2 dx$ and $\mathcal{I}_{2\pm} = \int e^{\pm 2iq_cx}|\psi(x,t)|^2 dx$ quantify the ordering of atoms into the optical potential minima.

We find the stationary ground-state solution $e^{-i\mu_0 t}\psi_0(x)$ of Eqs. (18) by self-consistently solving the equations via setting $\partial_t\alpha_j = 0$ for $j = 0, \pm$ and $i\partial_t\psi = \mu\psi$ [28]. Neglecting the BEC medium boundary effects, the Λ_c periodicity of the optical potential arising from the cavity-photon modes in Eq. (5) allows us to solve the equations on a box of length Λ_c, applying periodic boundary conditions.

In Fig. 3 we compare the steady-state results for the three-mode model and the full system of equations (18). Both the sideband fields $\alpha_\pm^0$ and the integrals $\mathcal{I}_\pm^0$ and $\mathcal{I}_{2\pm}^0$ vanish below threshold. For pump rates $\eta \gtrsim \eta_c$, the quantities acquire finite values, which are approximately equal for the three-mode model and Eqs. (18). For these η values, both the electric-field intensity distributions and the probability distributions are also approximately equal for the two models. The three-mode model gives thus a very good approximation of the system behavior in this regime.

Increasing η higher above threshold, the modulation depth of the self-organized cavity-photon standing wave becomes quadratically larger, which can be seen from the inset of

Fig. 3(a) by noting that $I_0 \approx \eta^2/N/(\bar{\Delta}_c^2 + \kappa^2)$. The atoms are thus more strongly localized in the optical potential wells and their probability distribution $|\psi_0(x)|^2$ becomes noticeably different from the prediction for the three-mode approximation. This is also reflected in the increase of discrepancy of the $|\alpha_\pm^0|$, $|\mathcal{I}_\pm^0|$, and $|\mathcal{I}_{2\pm}^0|$ values for the two models. Including higher-order atomic momenta thus becomes necessary for quantitatively describing the steady-state system behavior for large η/η_c values.

C. Collective excitation spectrum

We use here the Bogoliubov–de Gennes approach outlined in [28,54,60] to calculate the collective excitation spectrum. We consider solutions of the forms $\psi(x,t) = e^{-i\mu_0 t}[\psi_0(x) + \delta\psi(x,t)]$ and $\alpha_j(t) = \alpha_j^0 + \delta\alpha_j(t)$, where $\delta\psi(x,t) = \delta\psi^+(x)e^{-i\Omega t} + [\delta\psi^-(x)]^*e^{i\Omega^* t}$ and $\delta\alpha_j(t) = \delta\alpha_j^+ e^{-i\Omega t} + (\delta\alpha_j^-)^*e^{i\Omega^* t}$ for $j = 0, \pm$. Inserting these relations into Eqs. (18) and collecting the $e^{-i\Omega t}$ and $e^{i\Omega^* t}$ terms, the collective excitation spectrum is now determined by the eigenvalue equation

$$\hat{M}\mathbf{R} = \Omega\mathbf{R}, \qquad (19)$$

with the non-Hermitian excitation matrix $\hat{M}$ given by Eq. (C3) and the excitation vector defined as

$$\mathbf{R} = [\delta\alpha_0^+, \delta\alpha_0^-, \delta\alpha_+^+, \delta\alpha_+^-, \delta\alpha_-^+, \delta\alpha_-^-, \delta\psi^+(x), \delta\psi^-(x)]^\top. \qquad (20)$$

We numerically calculate the spectrum of $\hat{M}$ by using a spatial grid of length Λ_c with 256 points and periodic boundary conditions. Due to the symmetry properties of $\hat{M}$, its eigenvalues appear in pairs with equal imaginary parts and real parts with opposite signs [54,60]; we plot here only the part of the spectrum with positive real parts.

In Fig. 4 we plot the first six eigenvalues of $\hat{M}$ for scanning η, excluding the zero-frequency mode, which gives rise to phase diffusion of the homogeneous part of the condensate for all η [61]. At $\eta \ll \eta_c$, the collective condensate mode pairs have frequencies ω_R, $4\omega_R$, and $9\omega_R$, which correspond to the spectrum of a condensate in a box [60]. The lowest-energy cavity-photon modes have, for the parameters used, a frequency of approximately $-\bar{\Delta}_c' = 89\omega_R$, which is not within the range of the plot.

Near the self-organization threshold pump rate η_c, the two lowest mode frequencies approach zero, and moving beyond η_c leads to the splitting of the modes into a gapless mode, indicating a phase (Goldstone) mode, and a mode with a finite-energy gap. The frequency of the finite-gap mode vanishes for $\eta \to \eta_c$, indicating an amplitude (Higgs) mode excitation with fluctuations in the strength of the atomic density modulation [55]. The simultaneous presence of Goldstone and Higgs modes in the collective excitation spectrum is a signature of BEC supersolidity [5,48]. In contrast to the model of [5,62], the continuous translational symmetry here is exact such that no finite gap appears for the Goldstone mode.

Note that the cavity-photon decay with rate κ may cause finite values of the decay rates $-\mathrm{Im}(\Omega)$ of the collective excitations. However, for the Goldstone mode the decay rate is finite only for $\eta < \eta_c$ and the damping vanishes above threshold (see the inset of Fig. 4). This can be explained by the fact
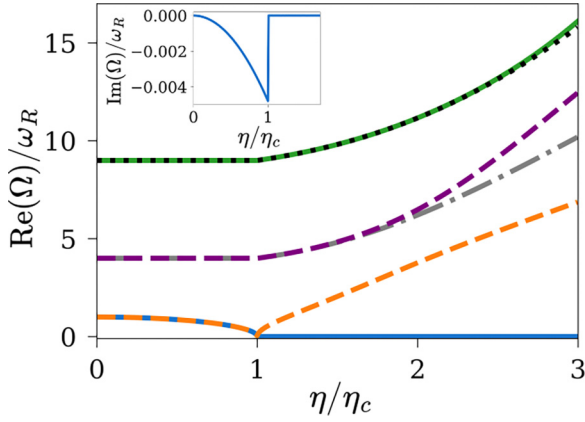
FIG. 4. Real parts of the six lowest eigenvalues of the collective excitation matrix $\hat{M}$ vs pump rate η. The plotted modes represent condensate density excitations at frequencies ω_R, $4\omega_R$, and $9\omega_R$ for $\eta \ll \eta_c$, and the lowest-energy photon modes appear at $\mathrm{Re}(\Omega) = -\bar{\Delta}'_c = 89\omega_R$. Above threshold, one of the two lowest modes becomes gapless (blue solid line), indicating Goldstone mode behavior, while the other mode obtains an energy gap increasing with η (orange dashed line), indicating Higgs mode behavior, as a direct consequence of spontaneous breaking of the U(1) translational symmetry of the Hamiltonian $\hat{H}_{\mathrm{eff}}$ by self-organization [5,48]. The inset shows that the decay rate $-\mathrm{Im}(\Omega)$ of the Goldstone mode vanishes above threshold, as a consequence of the fact that the continuous translational symmetry of the system equations is not broken by cavity-photon decay at rate κ. The simulation parameters are given in the caption of Fig. 3.

that cavity-photon decay does not break the U(1) translational symmetry of the Lindblad evolution equations for the photon modes [53] such that finite κ will not dampen the Goldstone mode appearing after spontaneous symmetry breaking of U(1) translational symmetry in the thermodynamic limit. The same feature is also present in the model studied in [44].

IV. COMMENSURATE AND INCOMMENSURATE MODES IN A MULTIMODE CAVITY

The great majority of work on quantum simulation with atoms coupled to optical resonators has involved coupling to a single or two cavity modes, which gives rise to global interaction between the atoms [2]. However, many of the Hamiltonians of interest to the condensed-matter physics community, such as models of the glassy phase [63–65] or frustrated magnetism [66], rely on more exotic types of interaction.

We study here a simple example where the effective atom-atom interaction has a more complex spatial profile compared to the global interaction case described in the preceding section. This modification is achieved by tailoring the distribution of multiple sideband modes circulating inside the cavity. The Gross-Pitaevskii-type equation for the atoms is now given by

$$i\frac{\partial\psi}{\partial t} = -\frac{1}{2m}\frac{\partial^2\psi}{\partial x^2} + V_1(x)\psi$$

$$+ u_0\Bigg(|\alpha_0|^2 + \sum_{q_j \in S}[|\alpha_{j+}|^2 + |\alpha_{j-}|^2$$

$$+ (\alpha_0^*\alpha_{j-} + \alpha_{j+}^*\alpha_0)e^{-iq_jx} + \alpha_{j+}^*\alpha_{j-}e^{-2iq_jx}$$

$$+ (\alpha_0^*\alpha_{j+} + \alpha_{j-}^*\alpha_0)e^{iq_jx} + \alpha_{j-}^*\alpha_{j+}e^{2iq_jx}]\Bigg)\psi, \quad (21)$$

where $V_1(x)$ is an external box-shaped potential, which leads to hard-wall boundary conditions for $\psi(x)$ at the edges of the system. As the on-axis mode is driven by a pump laser, we approximate it here by $\alpha_0 \simeq i\eta/\sqrt{N}(\bar{\Delta}_c + i\kappa)$ (see Appendix B). For large κ and/or $|\bar{\Delta}_{c,j}|$, and $|\Delta_a|$ values, sideband modes can then be adiabatically eliminated and approximated by

$$\alpha_{j\pm} \simeq \frac{U_0\alpha_0}{\bar{\Delta}_{c,j} + i\kappa} \int e^{\mp iq_jx}|\psi(x)|^2dx, \quad (22)$$

as also shown in Appendix B.

For the configurations studied here, nine cavity modes are selected by Fourier filtering. In the first example, the wave numbers are commensurate and given by $q_j = (1, 0.5, 0.25, 0.125)q_c$. The probability distribution for a realization of the ground-state wave function $\psi_0(x)$ is shown in Fig. 5(a). For these commensurate transverse wavelengths, the sideband cavity modes constructively interfere at length scales of $8\Lambda_c$, which is also the periodicity of the minima of the atom-atom interaction profile $V_2(x, x')$. The atoms can thus order into a droplet array of periodicity $8\Lambda_c$, which simultaneously increases the diffraction into all of the allowed cavity modes and minimizes the atomic potential energy.

In contrast, when the modes are incommensurate, such ordering in $\psi_0(x)$ does not occur, as shown in the example in Fig. 5(b), where $q_j = (1, 0.775, 0.575, 0.225)q_c$. Here a single constructive interference peak between all of the allowed modes occurs for $|x - x'| = 0$. It is thus not possible to simultaneously enhance the scattering into all cavity modes for atoms arranged in a periodic array. The ground-state solution is now a single-droplet state. Detunings $\Delta_{c,j}$ depend on the diffractive phase shifts of the sideband modes propagating in the system [12,53]. In Fig. 5 we plot the case for which $\bar{\Delta}_{c,j}$ is equal for all sidebands and the case for which $\bar{\Delta}_{c,j}$ depends on q_j. For the latter case, near cavity degeneracy the quadratic relationship $\omega_{c,j} - \omega_0 \propto q_j^2$ holds [21,53], which is used here to determine the detunings $\bar{\Delta}_{c,j}$. The two cases have the same ground-state solutions. The depth of the $V_2(x, x')$ minima is larger for the parameters of the case with variable $\bar{\Delta}_{c,j}$ such that the localization of the atoms at the optical potential minima is stronger here. Using wave-front-shaping elements inside the cavity feedback loop, the cavity sideband phase shifts can be controlled in order to tailor the distribution of $\bar{\Delta}_{c,j}$ values and, in combination with selecting the q_j distribution, engineer the shape of $V_2(x, x')$, which is an intriguing prospect for applications in quantum simulation.

V. CONCLUSION

A method for providing tailored photon-mediated atom-atom interaction in a BEC was studied theoretically and numerically. The method is based on diffractive coupling by electromagnetic modes of a ring cavity. In the first example of self-organization into stripe states, it was shown how the continuous translational symmetry of the system
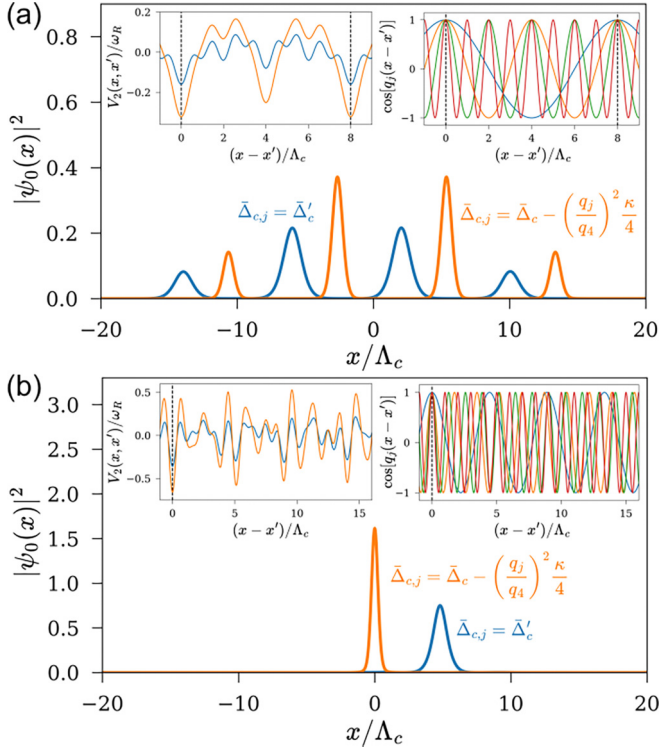
FIG. 5. Results for a multimode cavity with nine cavity modes. (a) Plot of $|\psi_0|^2$ for commensurate cavity modes with $q_j = (1, 0.5, 0.25, 0.125)q_c$ (blue, constant $\bar{\Delta}_{c,j}$; orange, variable $\bar{\Delta}_{c,j}$). (b) Plot of $|\psi_0|^2$ for incommensurate cavity modes with $q_j = (1, 0.775, 0.575, 0.225)q_c$ (blue, constant $\bar{\Delta}_{c,j}$; orange, variable $\bar{\Delta}_{c,j}$). The left inset shows the atom-atom interaction profile $V_2(x, x')$ with $U_0 \to u_0$ (blue, constant $\bar{\Delta}_{c,j}$; orange, variable $\bar{\Delta}_{c,j}$). The right inset shows cosine functions for modes with different q_j values (red, q_1; green, q_2; orange, q_3; blue, q_4). The simulation parameters are $(\bar{\Delta}_c, \bar{\Delta}'_c, u_0, \kappa) = (3, -2, -0.1, 20)\omega_R$ and (a) $\eta = 290\omega_R$ (blue) and $\eta = 270\omega_R$ (orange) and (b) $\eta = 430\omega_R$ (blue) and $\eta = 350\omega_R$ (orange). For constant $\bar{\Delta}_{c,j}$ the value is $\bar{\Delta}_{c,j} = \bar{\Delta}'_c$. For variable $\bar{\Delta}_{c,j}$ the value is changed as $\bar{\Delta}_{c,j} = \bar{\Delta}_c - (q_j/q_4)^2\kappa/4$. Hard-wall boundary conditions were imposed at the system ends at $x = \pm 20$.

Hamiltonian is manifested in the sombrero shape of the effective mean-field potential for the atomic degrees of freedom above the self-organization threshold. This symmetry is spontaneously broken in the thermodynamic limit, by the system selecting a particular phase for the steady-state sinusoidal pattern in the atomic density and intracavity light field profile. Supersolid properties are exhibited by the simultaneous presence of Goldstone and Higgs modes in the numerically calculated collective excitation spectrum. The calculations corroborate previous remarks regarding supersolidity of optomechanical patterns in a BEC, observed for simulations in the single retroreflecting mirror configuration [10], which is a setup similar to the ring cavity scheme [12]. It should be readily possible to extend the problem into two-dimensional geometries, where an additional rotational U(1) symmetry will be broken by self-organization, which relates to the recent interest in supersolidity of dipolar condensates in two dimensions [49,50].

For highly elongated clouds [67,68], spatial features can be tuned to values of tens of microns, which would enable real space monitoring of the condensate dynamics. This also opens the possibility of modifying the photon-mediated interatomic interaction by placing optical elements with spatially tailored profiles within the optical feedback loop of the cavity.

Going beyond global all-to-all atom-atom coupling occurring for three cavity modes, we also studied the case of a multimode cavity with a tailored distribution of photonic sidebands. For commensurate transverse wave numbers q_j, the ground state is a droplet array, which simultaneously enhances scattering into all of the allowed cavity modes. In contrast, for incommensurate modes only one atom-atom potential minimum occurs, at $|x - x'| = 0$. The resulting ground-state solution is a single-droplet state. These example situations demonstrate the versatility of the proposed experimental setup. A wide variety of interaction profiles $V_2(x, x')$ can be implemented in this context, which may lead to nonequilibrium realizations of models of spin glasses [63–65] or frustrated magnetism [66].

APPENDIX A: DERIVATION OF THE EFFECTIVE HAMILTONIAN

The effective Hamiltonian (2) can be derived from the Jaynes-Cummings model, similarly to the procedure given in Refs. [28,70]. We describe the atom-light interaction within the domain of paraxial approximation, where only forward-directed scattering of light by the condensate can occur, such that only counterclockwise- or clockwise-propagating modes can be excited by the instability. We can thus concentrate on a one-dimensional model, where the cavity-mode operator at the BEC medium is

given by

$$\hat{E}(x) = \hat{a}_0 + \sum_{q_j \in S}(\hat{a}_{j+}e^{iq_j x} + \hat{a}_{j-}e^{-iq_j x}), \tag{A1}$$

where $\hat{a}_0$ is the annihilation operator of the on-axis plane wave mode and $\hat{a}_{j\pm}$ are the annihilation operators of the diffracted sidebands with transverse wave numbers $\pm q_j = \pm 2\pi/\Lambda_j$. The allowed sideband wave numbers q_j are part of a bounded discrete set S, and the values contained within S can be experimentally tailored via Fourier filtering [15,30].

In the dipole and rotating-wave approximations, the single-atom Jaynes-Cummings Hamiltonian of the system is given by ($\hbar = 1$)

$$\hat{\mathcal{H}}^{(1)} = -\frac{1}{2m}\frac{\partial^2}{\partial x^2} + \omega_a \hat{\sigma}_{ee} + \left[\left(g_0 \hat{a}_0 + \sum_{q_j \in S} g_j(\hat{a}_{j+}e^{iq_j x} + \hat{a}_{j-}e^{-iq_j x})\right)\hat{\sigma}_{eg} + \text{H.c.}\right]$$

$$+ V_e(x)\hat{\sigma}_{ee} + V_g(x)\hat{\sigma}_{gg} + \omega_0 \hat{a}_0^\dagger \hat{a}_0 + \sum_j \omega_j(\hat{a}_{j+}^\dagger \hat{a}_{j+} + \hat{a}_{j-}^\dagger \hat{a}_{j-}) + i\eta(\hat{a}_0^\dagger e^{-i\omega t} - \hat{a}_0 e^{i\omega t}), \tag{A2}$$

where m is the mass of the atom; ω_a, ω, and ω_j are the frequencies of the atomic two-level transition, the drive laser, and the jth cavity mode, respectively; g_j is the atom-cavity coupling strength of the jth mode; $\hat{\sigma}_{kk'} = |k\rangle\langle k'|$ is the atomic optical transition operator; $V_{g,e}(x)$ are the external trapping potentials for atoms in the ground and excited states, respectively; $\eta \in \mathbb{R}$ is the laser pump rate; and the sum over j implies Fourier filtering of q_j was performed. In the following we approximate all g_j values by $g_0 \in \mathbb{R}$. Note that here we approximate the direct atom-atom scattering in the BEC to be sufficiently small to be neglected, i.e., the phenomena studied in this article are based only on photon-mediated interaction between the atoms.

The Hamiltonian (A2) can be converted into a time-independent form

$$\hat{\tilde{\mathcal{H}}}^{(1)} = \hat{U}\hat{\mathcal{H}}^{(1)}\hat{U}^\dagger + i(\partial_t \hat{U})\hat{U}^\dagger$$

$$= -\frac{1}{2m}\frac{\partial^2}{\partial x^2} - \Delta_a \hat{\sigma}_{ee} + [g_0 \hat{E}(x)\hat{\sigma}_{eg} + \text{H.c.}] + V_e(x)\hat{\sigma}_{ee} + V_g(x)\hat{\sigma}_{gg} - \Delta_c \hat{a}_0^\dagger \hat{a}_0 - \sum_j \Delta_{c,j}(\hat{a}_{j+}^\dagger \hat{a}_{j+} + \hat{a}_{j-}^\dagger \hat{a}_{j-}) + i\eta(\hat{a}_0^\dagger - \hat{a}_0),$$

$$\tag{A3}$$

where $\Delta_a = \omega - \omega_a$, $\Delta_c = \omega - \omega_0$, and $\Delta_{c,j} = \omega - \omega_j$, by using

$$\hat{U} = \exp\left[i\omega t\left(\hat{\sigma}_{ee} + \hat{a}_0^\dagger \hat{a}_0 + \sum_j(\hat{a}_{j+}^\dagger \hat{a}_{j+} + \hat{a}_{j-}^\dagger \hat{a}_{j-})\right)\right]. \tag{A4}$$

The corresponding many-body Hamiltonian of the system is given by

$$\hat{H} = \int \hat{\Psi}_g^\dagger(x)\left(-\frac{1}{2m}\frac{\partial^2}{\partial x^2} + V_g(x)\right)\hat{\Psi}_g(x)dx + \int \hat{\Psi}_e^\dagger(x)\left(-\frac{1}{2m}\frac{\partial^2}{\partial x^2} + V_e(x) - \Delta_a\right)\hat{\Psi}_e(x)dx$$

$$+ \int [g_0 \hat{\Psi}_e^\dagger(x)\hat{E}(x)\hat{\Psi}_g(x) + \text{H.c.}]dx - \Delta_c \hat{a}_0^\dagger \hat{a}_0 - \sum_j \Delta_{c,j}(\hat{a}_{j+}^\dagger \hat{a}_{j+} + \hat{a}_{j-}^\dagger \hat{a}_{j-}) + i\eta(\hat{a}_0^\dagger - \hat{a}_0), \tag{A5}$$

where

$$[\hat{\Psi}_k(x), \hat{\Psi}_{k'}^\dagger(x')] = \delta(x - x')\delta_{k,k'},$$
$$[\hat{\Psi}_k(x), \hat{\Psi}_{k'}(x')] = [\hat{\Psi}_k^\dagger(x), \hat{\Psi}_{k'}^\dagger(x')] = 0. \tag{A6}$$

The Heisenberg equation for $\hat{\Psi}_e(x)$ is given by

$$i\frac{\partial \hat{\Psi}_e(x)}{\partial t} = \left(-\frac{1}{2m}\frac{\partial^2}{\partial x^2} + V_e(x) - \Delta_a\right)\hat{\Psi}_e(x) + g_0 \hat{E}(x)\hat{\Psi}_g(x). \tag{A7}$$

In the limit of large Δ_a, the excited-state dynamics reaches steady state much more quickly than the ground state. The kinetic energy and external potential terms can be neglected in comparison to Δ_a, and $\hat{\Psi}_e(x)$ can be adiabatically eliminated to give

$$\hat{\Psi}_e(x) \simeq \frac{1}{\Delta_a}g_0 \hat{E}(x)\hat{\Psi}_g(x). \tag{A8}$$

The Heisenberg equations for the cavity operators $\hat{a}_0$ and $\hat{a}_j$ (including a phenomenological cavity decay constant κ) and the atomic field $\hat{\Psi}_g(x) \equiv \hat{\psi}(x)$ can be derived from (A5), which after inserting (A8) leads to

$$\frac{\partial \hat{a}_0}{\partial t} = (i\Delta_c - \kappa)\hat{a}_0 - iU_0 \int \hat{\psi}^{\dagger}(x)\hat{E}(x)\hat{\psi}(x)dx + \eta,$$

$$\frac{\partial \hat{a}_{j\pm}}{\partial t} = (i\Delta_{c,j} - \kappa)\hat{a}_{j\pm} - iU_0 \int \hat{\psi}^{\dagger}(x)\hat{E}(x)e^{\mp iq_j x}\hat{\psi}(x)dx,$$

$$\frac{\partial \hat{\psi}(x)}{\partial t} = \left(-\frac{1}{2m}\frac{\partial^2}{\partial x^2} + V_1(x) + U_0\hat{E}^{\dagger}(x)\hat{E}(x)\right)\hat{\psi}(x). \tag{A9}$$

Equations (A9) can be derived from the Heisenberg equation with the effective Hamiltonian $\hat{H}_{\text{eff}}$ given by

$$\hat{H}_{\text{eff}} = -\Delta_c \hat{a}_0^{\dagger}\hat{a}_0 - \sum_j \Delta_{c,j}(\hat{a}_{j+}^{\dagger}\hat{a}_{j+} + \hat{a}_{j-}^{\dagger}\hat{a}_{j-}) + i\eta(\hat{a}_0^{\dagger} - \hat{a}_0)$$

$$+ \int \hat{\psi}^{\dagger}(x)\left(-\frac{1}{2m}\frac{\partial^2}{\partial x^2} + V_1(x) + U_0\hat{E}^{\dagger}(x)\hat{E}(x)\right)\hat{\psi}(x)dx. \tag{A10}$$

APPENDIX B: PHOTON-MEDIATED INTERATOMIC INTERACTION

In the limit of large $|\Delta_{c,j}|$ and/or κ, the cavity-photon operators can be adiabatically eliminated. The system can then be described by a Hamiltonian of the form

$$\hat{H}_{\text{eff,at}} = \int \hat{\psi}^{\dagger}(x)\left(-\frac{1}{2m}\frac{\partial^2}{\partial x^2} + V_1(x)\right)\hat{\psi}(x)dx + \frac{1}{2}\int \hat{\psi}^{\dagger}(x')\hat{\psi}^{\dagger}(x)V_2(x,x')\hat{\psi}(x)\hat{\psi}(x')dx\,dx', \tag{B1}$$

where $V_2(x,x')$ is the effective atom-atom interaction mediated by cavity photons.

To determine the form of $V_2(x,x')$, we first adiabatically eliminate the on-axis mode, which leads to

$$\hat{a}_0 \simeq \frac{i\eta}{\bar{\Delta}_c + i\kappa} + O\left(\frac{1}{\Delta_a}\right), \tag{B2}$$

where $\bar{\Delta}_c = \omega - \omega_0 - NU_0$ and we neglect the terms $O(1/\Delta_a)$. As the on-axis mode is driven by a laser, one can approximate $\hat{a}_0$ by $\langle \hat{a}_0 \rangle \rightarrow \sqrt{N}\alpha_0$, where $\alpha_0 \simeq i\eta/\sqrt{N}(\bar{\Delta}_c + i\kappa)$ [53]. The sideband cavity-photon operators can then be adiabatically eliminated to give

$$\hat{a}_{j\pm} \simeq \frac{U_0\sqrt{N}\alpha_0}{\bar{\Delta}_{c,j} + i\kappa} \int e^{\mp iq_j x}\hat{\psi}^{\dagger}(x)\hat{\psi}(x)dx + O\left(\frac{1}{\Delta_a^2}\right), \tag{B3}$$

where $\bar{\Delta}_{c,j} = \omega - \omega_j - NU_0$ and we neglect the $O(1/\Delta_a^2)$ terms. Inserting expressions (B2) and (B3) into the Heisenberg equation (A9) for $\hat{\psi}(x)$ leads to

$$\frac{\partial \hat{\psi}(x)}{\partial t} = \left(-\frac{1}{2m}\frac{\partial^2}{\partial x^2} + V_1(x) + \int \hat{\psi}^{\dagger}(x')V_2(x,x')\hat{\psi}(x')dx'\right)\hat{\psi}(x), \tag{B4}$$

where the atom-atom interaction is given by

$$V_2(x,x') = \frac{\eta^2}{\bar{\Delta}_c^2 + \kappa^2}\left(\frac{U_0}{N} + 4U_0^2\sum_{q_j \in S}\frac{\bar{\Delta}_{c,j}}{\bar{\Delta}_{c,j}^2 + \kappa^2}\cos[q_j(x-x')]\right), \tag{B5}$$

and the constant first term in (B5) can be neglected. An effective atom-only Hamiltonian for this case is then given by Eq. (B1).

APPENDIX C: EXCITATION MATRIX $\hat{M}$

Inserting $\psi(x,t) = e^{-i\mu_0 t}[\psi_0(x) + \delta\psi(x,t)]$ and $\alpha_j(t) = \alpha_j^0 + \delta\alpha_j(t)$, for $j = 0, \pm$, into Eqs. (18), the dynamical equations are

$$\frac{\partial \delta\alpha_0}{\partial t} = (i\bar{\Delta}_c - \kappa)\delta\alpha_0 - iu_0\left(\mathcal{I}_+^0\delta\alpha_+ + \mathcal{I}_-^0\delta\alpha_- + \int A_0(\psi_0\delta\psi^* + \psi_0^*\delta\psi)dx\right),$$

$$\frac{\partial \delta\alpha_\pm}{\partial t} = (i\bar{\Delta}_c' - \kappa)\delta\alpha_\pm - iu_0\left(\mathcal{I}_\mp^0\delta\alpha_0 + \mathcal{I}_{2\mp}^0\delta\alpha_\mp + \int A_\pm(\psi_0\delta\psi^* + \psi_0^*\delta\psi)dx\right),$$

$$i\frac{\partial \delta\psi}{\partial t} = (\mathcal{H}_0 - \mu_0)\delta\psi + u_0\psi_0(A_0\delta\alpha_0^* + A_0^*\delta\alpha_0 + A_+\delta\alpha_+^* + A_+^*\delta\alpha_+ + A_-\delta\alpha_-^* + A_-^*\delta\alpha_-), \tag{C1}$$

where $A_0 = \alpha_+^0 e^{iq_c x} + \alpha_-^0 e^{-iq_c x}$, $A_\pm = \alpha_0^0 e^{\mp iq_c x} + \alpha_\mp^0 e^{\mp 2iq_c x}$, and the Hamiltonian $\mathcal{H}_0$ is given by

$$\mathcal{H}_0 = -\frac{1}{2m}\frac{\partial^2}{\partial x^2} + u_0\big\{\big[(\alpha_0^0)^*\alpha_+^0 + (\alpha_-^0)^*\alpha_0^0\big]e^{iq_c x} + \big[(\alpha_0^0)^*\alpha_-^0 + (\alpha_+^0)^*\alpha_0^0\big]e^{-iq_c x} + (\alpha_-^0)^*\alpha_+^0 e^{2iq_c x} + (\alpha_+^0)^*\alpha_-^0 e^{-2iq_c x}\big\}. \quad (C2)$$

Writing $\delta\psi(x,t) = \delta\psi^+(x)e^{-i\Omega t} + [\delta\psi^-(x)]^* e^{i\Omega^* t}$ and $\delta\alpha_j(t) = \delta\alpha_j^+ e^{-i\Omega t} + (\delta\alpha_j^-)^* e^{i\Omega^* t}$ and collecting the $e^{-i\Omega t}$ and $e^{i\Omega^* t}$ terms, we get the equations

$$\Omega\delta\alpha_0^+ = (-\bar{\Delta}_c - i\kappa)\delta\alpha_0^+ + u_0\bigg(\mathcal{I}_+^0\delta\alpha_+^+ + \mathcal{I}_-^0\delta\alpha_-^+ + \int A_0(\psi_0\delta\psi^- + \psi_0^*\delta\psi^+)dx\bigg),$$

$$\Omega\delta\alpha_0^- = (\bar{\Delta}_c - i\kappa)\delta\alpha_0^- - u_0\bigg((\mathcal{I}_+^0)^*\delta\alpha_+^- + (\mathcal{I}_-^0)^*\delta\alpha_-^- + \int A_0^*(\psi_0\delta\psi^- + \psi_0^*\delta\psi^+)dx\bigg),$$

$$\Omega\delta\alpha_+^+ = (-\bar{\Delta}_c' - i\kappa)\delta\alpha_+^+ + u_0\bigg(\mathcal{I}_-^0\delta\alpha_0^+ + \mathcal{I}_{2-}^0\delta\alpha_-^+ + \int A_+(\psi_0\delta\psi^- + \psi_0^*\delta\psi^+)dx\bigg),$$

$$\Omega\delta\alpha_+^- = (\bar{\Delta}_c' - i\kappa)\delta\alpha_+^- - u_0\bigg((\mathcal{I}_-^0)^*\delta\alpha_0^- + (\mathcal{I}_{2-}^0)^*\delta\alpha_-^- + \int A_+^*(\psi_0\delta\psi^- + \psi_0^*\delta\psi^+)dx\bigg),$$

$$\Omega\delta\alpha_-^+ = (-\bar{\Delta}_c' - i\kappa)\delta\alpha_-^+ + u_0\bigg(\mathcal{I}_+^0\delta\alpha_0^+ + \mathcal{I}_{2+}^0\delta\alpha_+^+ + \int A_-(\psi_0\delta\psi^- + \psi_0^*\delta\psi^+)dx\bigg),$$

$$\Omega\delta\alpha_-^- = (\bar{\Delta}_c' - i\kappa)\delta\alpha_-^- - u_0\bigg((\mathcal{I}_+^0)^*\delta\alpha_0^- + (\mathcal{I}_{2+}^0)^*\delta\alpha_+^- + \int A_-^*(\psi_0\delta\psi^- + \psi_0^*\delta\psi^+)dx\bigg),$$

$$\Omega\delta\psi^+ = (\mathcal{H}_0 - \mu_0)\delta\psi^+ + u_0\psi_0(A_0\delta\alpha_0^- + A_0^*\delta\alpha_0^+ + A_+\delta\alpha_+^- + A_+^*\delta\alpha_+^+ + A_-\delta\alpha_-^- + A_-^*\delta\alpha_-^+),$$

$$\Omega\delta\psi^- = -(\mathcal{H}_0 - \mu_0)\delta\psi^- - u_0\psi_0^*(A_0\delta\alpha_0^- + A_0^*\delta\alpha_0^+ + A_+\delta\alpha_+^- + A_+^*\delta\alpha_+^+ + A_-\delta\alpha_-^- + A_-^*\delta\alpha_-^+). \quad (C3)$$

Equation (C3) is an eigenvalue problem that can readily be written in matrix form $\hat{M}\mathbf{R} = \Omega\mathbf{R}$, where $\mathbf{R}$ is given by Eq. (20).

[1] H. Ritsch, P. Domokos, F. Brennecke, and T. Esslinger, Rev. Mod. Phys. **85**, 553 (2013).

[2] F. Mivehvar, F. Piazza, T. Donner, and H. Ritsch, Adv. Phys. **70**, 1 (2021).

[3] K. Baumann, C. Guerlin, F. Brennecke, and T. Esslinger, Nature (London) **464**, 1301 (2010).

[4] J. Léonard, A. Morales, P. Zupancic, T. Esslinger, and T. Donner, Nature (London) **543**, 87 (2017).

[5] J. Léonard, A. Morales, P. Zupancic, T. Donner, and T. Esslinger, Science **358**, 1415 (2017).

[6] S. C. Schuster, P. Wolf, S. Ostermann, S. Slama, and C. Zimmermann, Phys. Rev. Lett. **124**, 143602 (2020).

[7] Y. Guo, R. M. Kroeze, B. P. Marsh, S. Gopalakrishnan, J. Keeling, and B. L. Lev, Nature (London) **599**, 211 (2021).

[8] E. Tesio, G. R. M. Robb, T. Ackemann, W. J. Firth, and G.-L. Oppo, Phys. Rev. Lett. **112**, 043901 (2014).

[9] G. Labeyrie, E. Tesio, P. M. Gomes, G.-L. Oppo, W. J. Firth, G. R. M. Robb, A. S. Arnold, R. Kaiser, and T. Ackemann, Nat. Photon. **8**, 321 (2014).

[10] G. R. M. Robb, E. Tesio, G.-L. Oppo, W. J. Firth, T. Ackemann, and R. Bonifacio, Phys. Rev. Lett. **114**, 173903 (2015).

[11] Y.-C. Zhang, V. Walther, and T. Pohl, Phys. Rev. Lett. **121**, 073604 (2018).

[12] T. Ackemann, G. Labeyrie, G. Baio, I. Krešić, J. G. M. Walker, A. Costa Boquete, P. Griffin, W. J. Firth, R. Kaiser, G.-L. Oppo, and G. R. M. Robb, Atoms **9**, 35 (2021).

[13] I. Krešić, G. Labeyrie, G. R. M. Robb, G.-L. Oppo, P. M. Gomes, P. Griffin, R. Kaiser, and T. Ackemann, Commun. Phys. **1**, 33 (2018).

[14] G. Labeyrie, I. Krešić, G. R. M. Robb, G.-L. Oppo, R. Kaiser, and T. Ackemann, Optica **5**, 1322 (2018).

[15] G. Labeyrie, J. G. M. Walker, G. R. M. Robb, R. Kaiser, and T. Ackemann, Phys. Rev. Lett. **132**, 143402 (2024).

[16] L. A. Lugiato and R. Lefever, Phys. Rev. Lett. **58**, 2209 (1987).

[17] W. J. Firth, J. Mod. Opt. **37**, 151 (1990).

[18] W. J. Firth and C. Paré, Opt. Lett. **13**, 1096 (1988).

[19] E. Tesio, G. R. M. Robb, T. Ackemann, W. J. Firth, and G.-L. Oppo, Phys. Rev. A **86**, 031801(R) (2012).

[20] A. C. Boquete, G. Baio, G. Robb, G.-L. Oppo, P. Griffin, and T. Ackemann, J. Phys.: Conf. Ser. **1919**, 012014 (2021).

[21] A. Esteban-Martín, J. García, E. Roldán, V. B. Taranenko, G. J. de Valcárcel, and C. O. Weiss, Phys. Rev. A **69**, 033816 (2004).

[22] A. Esteban-Martín, V. B. Taranenko, J. García, G. J. de Valcárcel, and E. Roldán, Phys. Rev. Lett. **94**, 223903 (2005).

[23] M. Kreuzer, W. Balzer, and T. Tschudi, Appl. Opt. **29**, 579 (1990).

[24] K. Staliūnas, G. Šlekys, and C. O. Weiss, Phys. Rev. Lett. **79**, 2658 (1997).

[25] T. Ackemann, S. Barland, M. Cara, S. Balle, J. Tredicce, R. Jäger, M. Grabherr, M. Miller, and K. J. Ebeling, J. Opt. B **2**, 406 (2000).

[26] A. Periwal, E. S. Cooper, P. Kunkel, J. F. Wienand, E. J. Davis, and M. Schleier-Smith, Nature (London) **600**, 630 (2021).

[27] V. D. Vaidya, Y. Guo, R. M. Kroeze, K. E. Ballantine, A. J. Kollar, J. Keeling, and B. L. Lev, Phys. Rev. X **8**, 011002 (2018).

[28] N. Masalaeva, H. Ritsch, and F. Mivehvar, Phys. Rev. Lett. **131**, 173401 (2023).

[29] H. Tanji-Suzuki, I. D. Leroux, M. H. Schleier-Smith, M. Cetina, A. T. Grier, J. Simon, and V. Vuletić, in *Advances in Atomic, Molecular, and Optical Physics*, edited by E. Arimondo, P. R. Berman, and C. C. Lin (Elsevier, Amsterdam, 2011), Vol. 60, pp. 201–237.

[30] S. J. Jensen, M. Schwab, and C. Denz, Phys. Rev. Lett. **81**, 1614 (1998).

[31] A. F. Andreev and I. M. Lifshitz, Sov. Phys.-JETP **29**, 1107 (1969).

[32] G. V. Chester, Phys. Rev. A **2**, 256 (1970).

[33] A. J. Leggett, Phys. Rev. Lett. **25**, 1543 (1970).

[34] N. Prokof'ev and B. Svistunov, Phys. Rev. Lett. **94**, 155302 (2005).

[35] J. Toner, Phys. Rev. Lett. **100**, 035302 (2008).

[36] J. D. Reppy, Phys. Rev. Lett. **104**, 255301 (2010).

[37] M. Boninsegni and N. V. Prokof'ev, Rev. Mod. Phys. **84**, 759 (2012).

[38] D. Y. Kim and M. H. W. Chan, Phys. Rev. Lett. **109**, 155301 (2012).

[39] J. Xiang, C. Zhang, Y. Gao, W. Schmidt, K. Schmalzl, C.-W. Wang, B. Li, N. Xi, X.-Y. Liu, H. Jin *et al.*, Nature (London) **625**, 270 (2024).

[40] I. Bloch, J. Dalibard, and W. Zwerger, Rev. Mod. Phys. **80**, 885 (2008).

[41] A. J. Daley, I. Bloch, C. Kokail, S. Flannigan, N. Pearson, M. Troyer, and P. Zoller, Nature (London) **607**, 667 (2022).

[42] N. Bogoliubov, J. Phys. **11**, 23 (1947).

[43] S. Gopalakrishnan, B. L. Lev, and P. M. Goldbart, Phys. Rev. A **82**, 043612 (2010).

[44] F. Mivehvar, S. Ostermann, F. Piazza, and H. Ritsch, Phys. Rev. Lett. **120**, 123601 (2018).

[45] L. Chomaz, D. Petter, P. Ilzhöfer, G. Natale, A. Trautmann, C. Politi, G. Durastante, R. M. W. van Bijnen, A. Patscheider, M. Sohmen, M. J. Mark, and F. Ferlaino, Phys. Rev. X **9**, 021012 (2019).

[46] F. Böttcher, J.-N. Schmidt, M. Wenzel, J. Hertkorn, M. Guo, T. Langen, and T. Pfau, Phys. Rev. X **9**, 011051 (2019).

[47] L. Tanzi, S. Roccuzzo, E. Lucioni, F. Famà, A. Fioretti, C. Gabbanini, G. Modugno, A. Recati, and S. Stringari, Nature (London) **574**, 382 (2019).

[48] M. Guo, F. Böttcher, J. Hertkorn, J.-N. Schmidt, M. Wenzel, H. P. Büchler, T. Langen, and T. Pfau, Nature (London) **574**, 386 (2019).

[49] M. A. Norcia, C. Politi, L. Klaus, E. Poli, M. Sohmen, M. J. Mark, R. N. Bisset, L. Santos, and F. Ferlaino, Nature (London) **596**, 357 (2021).

[50] T. Bland, E. Poli, C. Politi, L. Klaus, M. A. Norcia, F. Ferlaino, L. Santos, and R. N. Bisset, Phys. Rev. Lett. **128**, 195302 (2022).

[51] A. Recati and S. Stringari, Nat. Rev. Phys. **5**, 735 (2023).

[52] J.-R. Li, J. Lee, W. Huang, S. Burchesky, B. Shteynas, F. C. Top, A. O. Jamison, and W. Ketterle, Nature (London) **543**, 91 (2017).

[53] I. Krešić, G. R. M. Robb, G.-L. Oppo, and T. Ackemann, Phys. Rev. Lett. **131**, 163602 (2023).

[54] G. Szirmai, D. Nagy, and P. Domokos, Phys. Rev. A **81**, 043639 (2010).

[55] D. Pekker and C. Varma, Annu. Rev. Condens. Matter Phys. **6**, 269 (2015).

[56] S. Coleman and E. Weinberg, Phys. Rev. D **7**, 1888 (1973).

[57] M. Kardar, *Statistical Physics of Fields* (Cambridge University Press, Cambridge, 2007).

[58] S. D. Bass, A. De Roeck, and M. Kado, Nat. Rev. Phys. **3**, 608 (2021).

[59] E. Tesio, G. R. M. Robb, G.-L. Oppo, P. M. Gomes, T. Ackemann, G. Labeyrie, R. Kaiser, and W. J. Firth, Philos. Trans. R. Soc. A **372**, 20140002 (2014).

[60] D. Nagy, G. Szirmai, and P. Domokos, Eur. Phys. J. D **48**, 127 (2008).

[61] D. Nagy, G. Szirmai, and P. Domokos, Phys. Rev. A **84**, 043637 (2011).

[62] J. Lang, F. Piazza, and W. Zwerger, New J. Phys. **19**, 123027 (2017).

[63] P. Strack and S. Sachdev, Phys. Rev. Lett. **107**, 277202 (2011).

[64] A. Angelone, F. Mezzacapo, and G. Pupillo, Phys. Rev. Lett. **116**, 135303 (2016).

[65] B. P. Marsh, R. M. Kroeze, S. Ganguli, S. Gopalakrishnan, J. Keeling, and B. L. Lev, Phys. Rev. X **14**, 011026 (2024).

[66] C.-L. Hung, A. González-Tudela, J. I. Cirac, and H. Kimble, Proc. Natl. Acad. Sci. USA **113**, E4946 (2016).

[67] J. H. V. Nguyen, D. Luo, and R. G. Hulet, Science **356**, 422 (2017).

[68] Y. Lim, J. Goo, H. Kwak, and Y. Shin, Phys. Rev. A **103**, 063319 (2021).

[69] S. Krämer, D. Plankensteiner, L. Ostermann, and H. Ritsch, Comput. Phys. Commun. **227**, 109 (2018).

[70] C. Maschler, I. B. Mekhov, and H. Ritsch, Eur. Phys. J. D **46**, 545 (2008).